# Analysis of spatiotemporal changes and driving factors of desertification in the Africa Sahel

Zuowei Yang [a,b], Xin Gao [a,b,*], Jiaqiang Lei [a,b], Xiaoyu Meng [a], Na Zhou [a,b]

[a] *State Key Laboratory of Desert and Oasis Ecology, Xinjiang Institute of Ecology and Geography, Chinese Academy of Sciences, 818 South Beijing Road, Urumqi 830011, Xinjiang, China*
[b] *University of Chinese Academy of Sciences, Beijing 100049, China*

A B S T R A C T

The transitional characteristics of desert grasslands in the Sahel determine the ecosystem's fragility, which is extremely susceptible to the expansion and reversal of land desertification under the influence of climate change and anthropogenic activities. Accordingly, monitoring desertification dynamics is essential to combat this process. Based on Moderate Resolution Imaging Spectroradiometer (MODIS) data, this study analysed the applicability of different feature space models to monitor desertification levels in the Sahel from 2000 to 2020, revealing the optimal monitoring model, analysing the spatiotemporal changes and primary driving factors. The results were as follows: In the Sahel, the albedo-modified soil adjusted vegetation index (MSAVI) based on the point-to-point model is the best for desertification monitoring, with an overall accuracy of 86.78%. Generally, the level of desertification was reduced from 2000 to 2020, the area of extremely severe desertification decreased by retreating northward; and the areas of light, moderate, and severe desertification increased slowly by expanding northward. Light, moderate, and severe desertification lands were more sensitive to climate change and anthropogenic activities, undergoing greater change intensity. Precipitation was the most influential factor determining the spatial distribution of desertification in the Sahel, with anthropogenic activities also having a significant effect on the desertification level. This study comprehensively analysed desertification patterns in the Sahel and identified the primary driving factors, which are essential to inform Sahelian desertification control mechanisms in the future.

## 1. Introduction

Desertification is a land degradation process in arid, semi-arid, and sub-humid areas resulting from climatic variations and unsustainable human economic activities (D'Odorico et al., 2013). As an important global ecological and socioeconomic problem, desertification not only causes the deterioration of ecological environment, but also reduces agricultural productivity and income (Cheng et al., 2018; Sterk and Stoorvogel, 2020). In recent years, global hotspot areas of desertification have expanded to 9.2% (±0.5%) of the arid area, affecting 500 million (±120 million) people (Mirzabaev et al., 2019). At present, the global surface is desertifying at a rate of 120,000 km$^2$·yr$^{-1}$, and it is estimated that by 2045, approximately 135 million people will be displaced by this process (Fust, 2010). Countries in the Sahel have proposed the Great Green Wall of Africa, which aims to eliminate land degradation by 2030. Berrahmouni et al. (2016) estimated that the recoverable degraded land

in the Sahel stands at 166 Mha, which requires a restoration rate of more than 10 Mha·yr$^{-1}$. However, up to now, more than 80% of the reforested trees have died (Benjaminsen and Hiernaux, 2019). The area of Lake Chad has shrunk by more than 90% from natural (e.g., drought) and anthropogenic factors, such as local population increase, reclamation of farmland, and large-scale irrigation (Policelli et al., 2019). The Horn of Africa has also shown clear trends towards drought from 1901 to 2010 (Tierney et al., 2015). All the situations further exacerbated desertification in the Sahel.

Over the past 30 years, researchers have found that the climate in the Sahel has become more humid, with increased vegetation and canopy coverage (Giannini et al., 2013; Brandt et al., 2020). Leroux et al. (2017) found that 16% of the Sahel has been re-greening. Comprehensive remote sensing data and field observation showed that vegetation restoration was obvious in the border area between Mali and Niger (Dardel et al., 2014). However, deforestation and bush destruction for
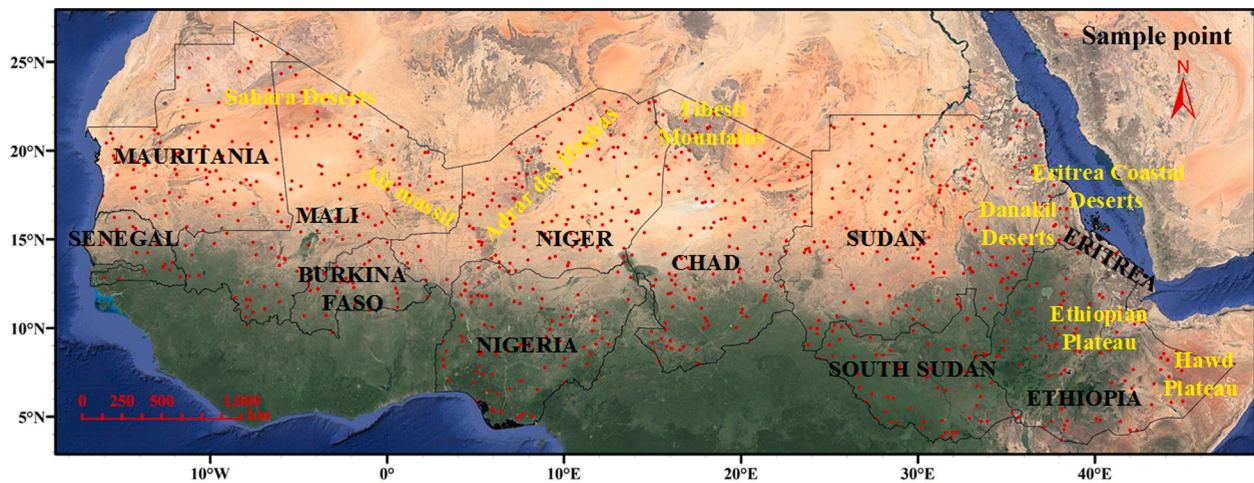
**Fig. 1.** Surface features of the Sahel and the sample point verifying desertification monitoring model. The base map is from Google Earth image.

firewood, raising livestock, and opening arable land have resulted in serious land degradation (Sop and Oldeland, 2013), and the lacking pace of reforestation has led to increased wind erosion and desertification in the Mauritania and Senegal regions (Niang et al., 2008; Rasmussen et al., 2018). Dimobe et al. (2015) reported that the arable land within the Total Wildlife Reserve of Bontioli (TWRB) in Burkina Faso has increased by 167.87%, and the natural vegetation land has decreased by 38.46% during 2001–2013. In the North Kurdufan State (Sudan), 120,000 km$^2$ of land has desertified; however, an increase in precipitation has improved the survival rate of afforestation, with vegetation regeneration covering approximately 200,000 km$^2$ of desertification land in the area (Dawelbait and Morari, 2012). Indeed, over the past few decades, there has been some controversy between re-greening and desertification in the Sahel (Kaptué et al., 2015; Kusserow, 2017). Therefore, it is of great practical significance to study the spatiotemporal changes of desertification in the Sahel over the recent 20 years. It can more clearly understand the level of desertification in different countries in the Sahel, the desertification control can be carried out in a targeted manner.

Remote sensing technology has provided researchers with novel method of monitoring desertification. Zeng et al. (2006) analysed the level of desertification by constructing an albedo-NDVI feature space, and calculating the desertification monitoring index (DMI) based on the results of linear fitting. This relatively simple method produced a higher accuracy than using spectral information alone for level division, and it has been applied to desertification assessments across different regions in recent years (Vorovencii, 2017; Li et al., 2021). In nonlinear situations of albedo-NDVI, Guo et al. (2020) proposed a point-to-point model based on distance. Since NDVI is highly influenced by soil background, it cannot accurately reflect the growth status of sparse vegetation (Kremer and Running, 1993); therefore, Qi et al. (1994) proposed the MSAVI, which accounts for the bare soil line, thus more thoroughly eliminating soil's spectral influence. Wu et al. (2019) established the albedo-MSAVI feature space model to analyse the degree of desertification of Inner Mongolia's grasslands. Further, the topsoil grain size index (TGSI) can characterise the mechanical composition of the surface soil and the level of desertification; for example, severe desertification corresponds to rough surfaced soil particles (Xiao et al., 2006). The Albedo-TGSI model is highly sensitive to surface soil changes and it can better extract information of severe and extremely severe desertification (Wei et al., 2018). Thus, in order to fully consider the vegetation coverage and surface roughness, a variety of surface parameters can be employed to construct DMIs based on linear and point-to-point models, respectively, to obtain the optimal monitoring model of desertification.

Additionally, determining and analysing the influential factors of the desertification process are an essential component of desertification control (Xu et al., 2011). Some studies have identified only soil or

vegetation conditions as factors leading to desertification (An et al., 2013; Turan et al., 2019), the Environmentally Sensitive Area Index (ESAI) can be constructed by collecting indicators affecting the desertification level in categories such as soil, climate, vegetation and management quality (Jiang et al., 2019; Uzuner and Dengiz, 2020). In order to clarify the impact of different driving factors on the level of desertification, most existing researches have analysed the correlation between desertification and various influential factors, or they have estimated the contribution of various influencing factors by using factor analysis and principal component analysis (Wang et al., 2006; Li et al., 2007; Xue et al., 2017). Additionally, the residual analysis method has been used to quantify the contributions of climate change and anthropogenic activities to desertification (Kundu et al., 2017). The geographical detector model proposed by Wang et al. (2016) only relied on the spatial heterogeneity of geographic variables and it did not involve any linear assumptions, which can not only quantitatively detect the main driving force of desertification level, but also quantitatively evaluate the driving force of the two influencing factors on the distribution of desertification level (Du et al., 2016; Hua and Hao, 2021). As the ecological environment of the Sahel is a fragile transitional zone between the desert and grasslands, it is very important to determine the dominant factors affecting desertification in this area, and any interactions among them.

This study was based on MODIS data containing several surface parameters, including NDVI, MSAVI, albedo, and TGSI, to construct a DMI based on a linear and point-to-point model for optimal desertification model in the Sahel. Using this best model, the level of desertification was monitored in the Sahel from 2000 to 2020, and the spatiotemporal evolution and intensity of change were further analysed. Finally, the main driving factors of desertification were identified by using a geographical detector model.

## 2. Material and methods

### 2.1. Study area

The Sahel stretches more than 5,900 km from the Atlantic Ocean to the Horn of Africa, extending across 11 countries, including Senegal, Mauritania, Mali, Burkina Faso, Niger, Nigeria, Chad, Sudan, South Sudan, Ethiopia, and Eritrea (Fig. 1). The climate of these countries is arid, with high temperatures and variable precipitation throughout the year, although it is primarily concentrated in the rainy season (June to September). The annual precipitation in the northern desert area is less than 100 mm; whereas the southern humid area can reach more than 1500 mm (Siebert, 2014). The highest temperatures were recorded from April to May, and the average maximum temperature can rise to 40to 42℃. The average minimum temperature decreased to 15℃ from
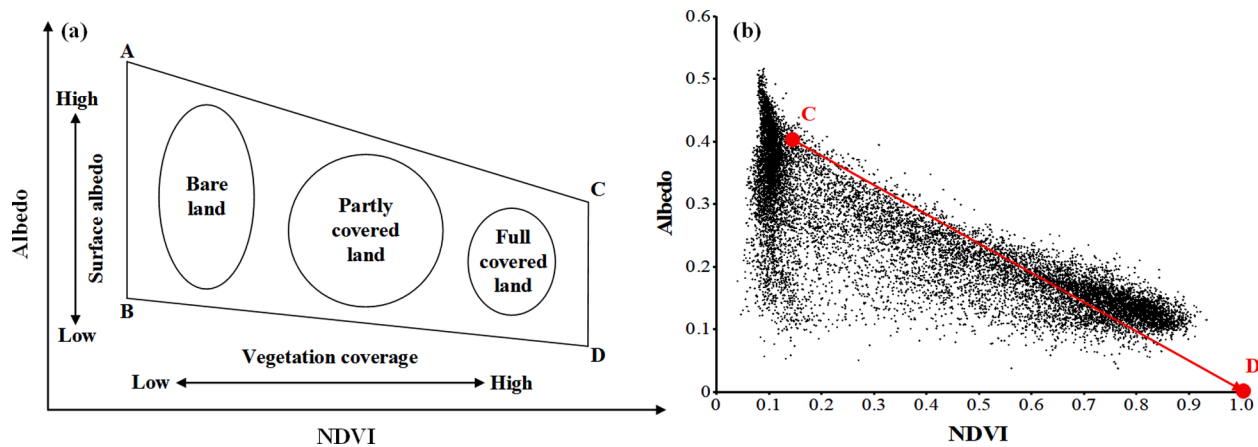
**Fig. 2.** Albedo-NDVI (a) feature space line plot and (b) scatter diagram (CD line refers to the distance from any point C in the feature space to the D (1, 0) with the best vegetation and the lowest albedo).

December to January. In some areas in the southwest of the Sahel, the temperatures were relatively low due to the cold ocean current brought by the Gulf of Guinea (Nicholson, 2018). The overall terrain of the Sahel is relatively flat, most of which are distributed between 200 to 500 meters, although the elevations of the Ethiopian Plateau and Tibesti Plateau are more than 3000 m, where large tracts of alpine grasslands and thickets exist (Houerou, 1980; Pye and White, 1985). The southern edge of the Sahara, resides in the northern part of the Sahel. The central transitional zone is a typical tropical savannah, and large tracts of farmland and forests are located at the southern end. The Sahel has the highest population growth rate in the world, and the regional livestock account for more than 25% of that found on the African continent (UNDP, 2019; Kamuanga et al., 2008). This massive population increase has driven a constant northward encroachment of dryland agriculture, and growing competition between animal husbandry and rainfed farming. Large numbers of livestock were crowded to the north, where sparse vegetation cover was highly susceptible to serious desertification under arid conditions (Hein and De Ridder, 2006).

### 2.2. Data collection and pre-processing

MODIS 8-day reflectance data (MOD09A1) was used to synthesise the maximum annual NDVI and MSAVI, and MODIS 16-day albedo product (MCD43A3) was used to synthesise the minimum annual albedo and TGSI (Table S1, Supplementary material). Both of them have a spatial resolution of 500 m. Different feature spaces are constructed based on the above four surface parameters, and DMIs based on linear and point-to-point models are calculated.

The occurrence and expansion of desertification are the products of the joint actions of natural and socioeconomic factors, where the former includes climate factors, topography factors, vegetation conditions, and soil conditions; whereas the latter mainly includes economic structure and land use types. Precipitation (PRE), temperature (TEM), potential evapotranspiration (PET), and wind speed (WS) were selected as the most influential climatic factors affecting desertification in the present study. Elevation (ELEV), slope (SLOP), and aspect (ASP) were selected here as the dominant topographic factors influencing desertification. It is also essential to define the desertification characteristics of different vegetation type (VT) and soil type (ST) for prevention and control mechanisms. Soil moisture (SM) has an important impact on vegetation distribution and growth. Animal husbandry is the primary economic industry in the Sahel, excessive livestock density (LD) can also lead to desertification. Land use type (LUT) changes are also closely related to desertification, and unsustainable land use, especially via reclamation and grazing in unsuitable areas. All driving factors (Table S2, Supplementary material) were resampled to a spatial resolution consistent with

TerraClimate data, facilitating the use of the geographical detector model for driving factor analysis (Fig. S1, Supplementary material).

### 2.3. Research methods

#### 2.3.1. Principles of feature space

When surface vegetation is severely damaged and coverage is dramatically reduced during land desertification, corresponding values of NDVI and MSAVI will decrease. Further, the reduction of vegetation coverage increases the albedo. Soil particle composition also becomes rougher with desertification, and the TGSI value increases correspondingly. Significant negative correlations have been found between albedo and NDVI in different desertification areas (Guo and Wen, 2020), and the albedo-NDVI feature space model proposed by Zeng et al. (2006) can be seen in Fig. 2a. The high albedo line (AC) indicates the level of land drought in the study area; whereas the low albedo line (BD) represents the maximum surface moisture condition (Fig. 2a). According to the research of Verstraete and Pinty (1996), it is possible to distinguish different degrees of desertification land by dividing the feature space in the vertical direction of the linear regression equation, and it can be expressed as the desertification monitoring index (DMI$_{LIN}$; Eq. (1)):

$$DMI_{LIN} = \alpha \times NDVI - Albedo \tag{1}$$

where $\alpha = 1/k$, $k$ is the slope of the trend line fit to by albedo and NDVI.

Based on the linear fitting results of the above two variables, most researchers have identified the levels of desertification in different regions by using the DMI$_{LIN}$ (Vorovencii, 2017; Li et al., 2021); however, when the albedo-NDVI relationship is nonlinear, this feature space model may not accurately reflect true desertification. To address this issue, Guo et al. (2020) proposed a point-to-point model based on distance from any point $C$ in the feature space, to point $D$ (1,0) with the best vegetation and the lowest albedo (Fig. 2b). This desertification monitoring index (DMI$_{P2P}$) was expressed according to Eq. (2):

$$DMI_{P2P} = \sqrt{(NDVI - 1)^2 + Albedo^2} \tag{2}$$

The average of DMI$_{P2P}$ from 2000 to 2020 was divided into five levels by using the natural breaks method: extremely severe, severe, moderate, light, and no desertification. Using this same method, the DMI of linear and point-to-point models based on the albedo-NDVI, albedo-MSAVI, TGSI-NDVI, and TGSI-MSAVI feature spaces were further established to extract information on Sahel desertification, and obtain an optimal monitoring model.

#### 2.3.2. Related methods of spatiotemporal changes

The levels of desertification in the Sahel from 2000 to 2020 were

**Table 1**
Types of two-factor interaction result.

| Description | Interaction |
|---|---|
| $q(X1 \cap X2) < \text{Min}(q(X1), q(X2))$ | Nonlinear-weaken |
| $\text{Min}(q(X1), q(X2)) < q(X1 \cap X2) < \text{Max}(q(X1), q(X2))$ | Uni-variable weaken- |
| $q(X1 \cap X2) > \text{Max}(q(X1), q(X2))$ | Bi-variable enhance |
| $q(X1 \cap X2) = q(X1) + q(X2)$ | Independent |
| $q(X1 \cap X2) > q(X1) + q(X2)$ | Nonlinear-enhance |

calculated according to the derived optimal monitoring model, and the dynamic evolution of the Sahel from 2000 to 2020 was explored by using an array of spatiotemporal analyses. The gravity centre model was initially used to calculate the centre coordinates of different desertification levels across certain time periods, thus reflecting the changes in corresponding spatial patterns (Na et al., 2019). A linear regression model based on the least squares method is a common in analyses of changing DMI trends (Gou et al., 2021; Hu et al., 2020). Pixel-by-pixel trend analyses of the desertification level was conducted, and a *t*-test was used to test the significance of changing DMI trends. Intensity analyses are an explanatory framework for the quantitative analysis of

changes between desertification levels based on a transition matrix, and it has three levels-interval, category, and transition-to explain the transformation mechanisms more clearly, and intuitively display the changing process of various types over different time periods (Aldwaik and Pontius, 2012). The specific introduction for the above-mentioned methods can be found in the Supplementary material.

*2.3.3. Geographical detector*

A geographical detector is a tool for detecting the spatially stratified heterogeneity of geographic elements, and identifying the driving forces behind it (Wang et al., 2016). Its central idea is that if independent variable *X* has an impact on dependent variable *Y*, the spatial distribution between them should be similar, and they can be measured by the *q* value (Eq. (3)):
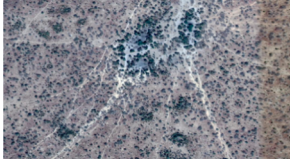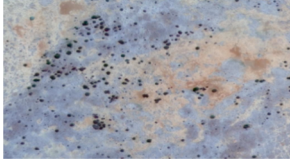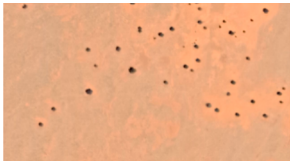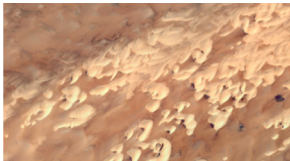
$$q = 1 - \frac{\sum_{h=1}^{L} Nh\sigma_h^2}{N\sigma^2} \tag{3}$$

where $h = 1, …, L$ are the strata of variable *Y* or factor *X*; the *N* and $N_h$ are the number of units in strata *h* and the whole area, respectively; $\sigma_h^2$
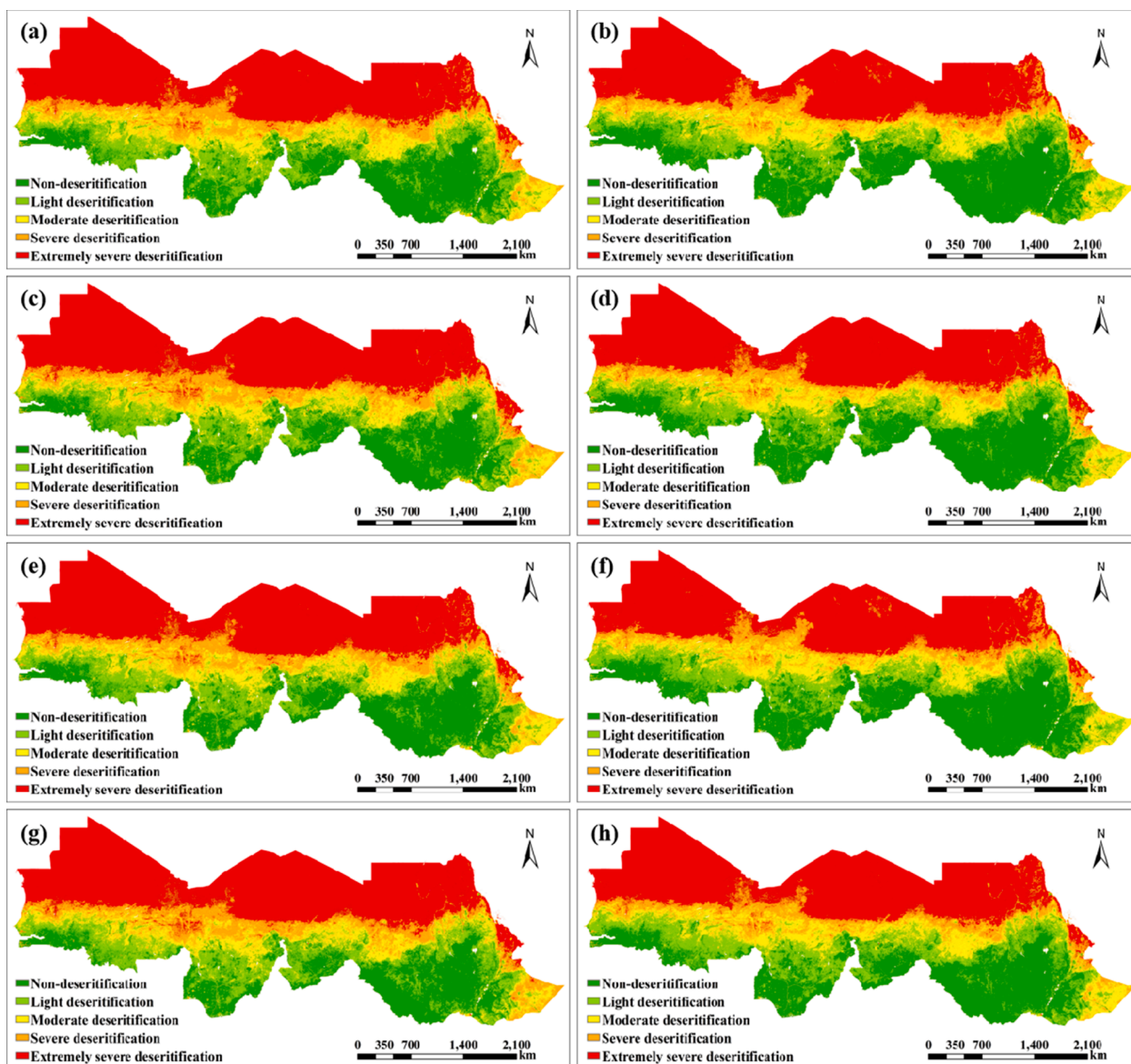


**Fig. 3.** Classification of desertification level based on eight feature spaces. Linear models: (a) Albedo-NDVI, (b) Albedo-MSAVI, (c) TGSI-NDVI, (d) TGSI-MSAVI; Point-to-point models: (e) Albedo-NDVI, (f) Albedo-MSAVI, (g) TGSI-NDVI, (h) TGSI-MSAVI.

**Table 2**

Classification criterion of desertification level.

| Desertification level | Interpretation in Google Earth image | Surface features |
|---|---|---|
| Non desertification |  | Forests, farmland, dense grasslands, etc., with high vegetation coverage. |
| Light desertification |  | Declining vegetation coverage, negatively affecting growth of native plant species. |
| Moderate desertification |  | Vegetation is distributed in patches, with degraded plants, and low shrub sand piles. |
| Severe desertification |  | Vegetation has nearly disappeared, with only a few shrubs or succulents. |
| Extremely severe desertification |  | Complete loss of land productivity, and regional vegetation disappearance, including bare lands, sandy lands, and Gobi. |

**Table 3**

Accuracy analyses of the different feature space models.

| Models | Albedo-MSAVI | Albedo-NDVI | TGSI-MSAVI | TGSI-NDVI |
|---|---|---|---|---|
| Linear | 85.67% | 73.78% | 83.44% | 72.33% |
| Point-to-point | 86.78% | 75.56% | 83.89% | 71.11% |

differences. To verify the accuracy of different DMI models in the Sahel, 900 sampling points were randomly selected throughout the study area (Fig. 1). According to the classification standards of existing studies (Han et al., 2010; Duan et al., 2019; Na et al., 2019), the desertification level of each sampling point was classified one by one in combination with Google Earth imagery in 2020 (Table 2). This formed the basis for verifying and comparing the monitoring results of the eight models in 2020. Overall classification accuracy was calculated according to a confusion matrix (Table 3), and the results showed that the MSAVI-TGSI and MSAVI-albedo models based on the point-to-point and the linear models had the overall accuracy of above 80%. In addition, the NDVI-albedo and NDVI-TGSI models based on the point-to-point and the linear models had the overall accuracy of above 70% as well. The MSAVI-albedo based on the point-to-point model had the highest accuracy of 86.78%. In general, the point-to-point models were more accurate than the linear models for monitoring desertification levels in the Sahel. MSAVI appeared to have effectively eliminated the influence of soil background.

### 3.2. Spatiotemporal variation of desertification

#### 3.2.1. Spatial variation

Based on the results of the model accuracy verification, the point-to-point albedo-MSAVI model was selected to calculate the DMI of the Sahel from 2000 to 2020. Fig. 4 shows the spatial distribution of different desertification levels in 2000, 2005, 2010, 2015, and 2020, revealing that extremely severe desertification was widely distributed, especially in the Sahara located to the north of the study area, as well as in the Danakil and Eritrea Coastal Deserts to the east. Severe desertification was concentrated in the semi-desert areas south of the Sahara, in addition to the Aïr massif and the Adrar des Ifoghas that extend northward into the Sahara. Moderate desertification was primarily located in the centre of the study area, where thickets are widespread, in addition to in the thorn bush and grassland areas in southeastern Ethiopia. Light desertification was mainly distributed in the savanna climate zone; whereas the forested area in the south, and dense alpine shrublands and grasslands on the Ethiopian Plateau comprised the non-desertification land. The areas of extremely severe desertification decreased over the analysis period, retreating to the north (Fig. 4). Alternatively, areas of severe, moderate, light, and non-desertification all extend to the north, particularly in the Aïr Massif of Niger, the Adrar des Ifoghas of Mali, and the Hawd Plateau in the southeastern corner of Ethiopia.

Fig. 5 shows the changes of all spatial gravity centres of desertification levels moving northward, consistent with the results shown in Fig. 4. The primary reason for the gravity centre shift of non-desertification land from the southwest to the northeast is the transition of a large land area in the southwest of Nigeria from non-desertification to light desertification; whereas the non-desertification land in the northeast of Ethiopia expanded northward. In terms of relevant conditions, the gravity centre of light desertification has migrated from the southeast to northwest. The gravity centre of moderate desertification has migrated from the southeast to northwest, driven by the decreasing level of desertification in the Tillaberi and Dosso regions of Niger. The gravity centre of severe desertification first shifted to the northwest, then to the east, and finally to the northeast due to the diminishing desertification of the Aïr Massif and Adrar des Ifoghas severe levels, prior to increasing again in 2015. The gravity centre of extremely severe desertification appeared to migrate northward, although randomly about the east-west direction.

and $\sigma^2$ are the variances of variable $Y$ in strata $h$ and the whole area, respectively; and $q$ ranges from [0,1], where larger values indicate a more obvious spatial differentiation of $Y$.

Geographical detectors are composed of four parts: factor, interactive, risk, and ecological detection. Factor detection can quantify the impact of each environmental factor on the distribution of DMIs, where higher $q$ values indicate greater impacts on DMI distribution. Interaction detection is used to determine the relationship between different influencing factors on the DMI (Table 1), and are further classified into five categories by comparing the $q$ value of a single factor ($q(X1)$, $q(X2)$), the sum of two single-factor $q$ values ($q(X1) + q(X2)$), and the $q$ value of the two-factor interaction ($q(X1 \cap X2)$). Risk detection is used to identify the influence of each environmental factor on DMI, and indicate their impact at different levels. Ecological detection is used to reveal any significant differences in the effects of any two influential factors, $X1$ and $X2$, on the spatial distribution of DMI, as measured by the $F$ statistics.

### 3. Results

#### 3.1. Desertification monitoring based on different characteristic spaces

Based on a thorough consideration of vegetation coverage and surface roughness, eight DMI models were constructed using four typical surface parameters: NDVI, MSAVI, albedo, and TGSI (Fig. 3). The resulting spatial distributions of desertification levels in the Sahel from these models were similar, albeit with some important localized
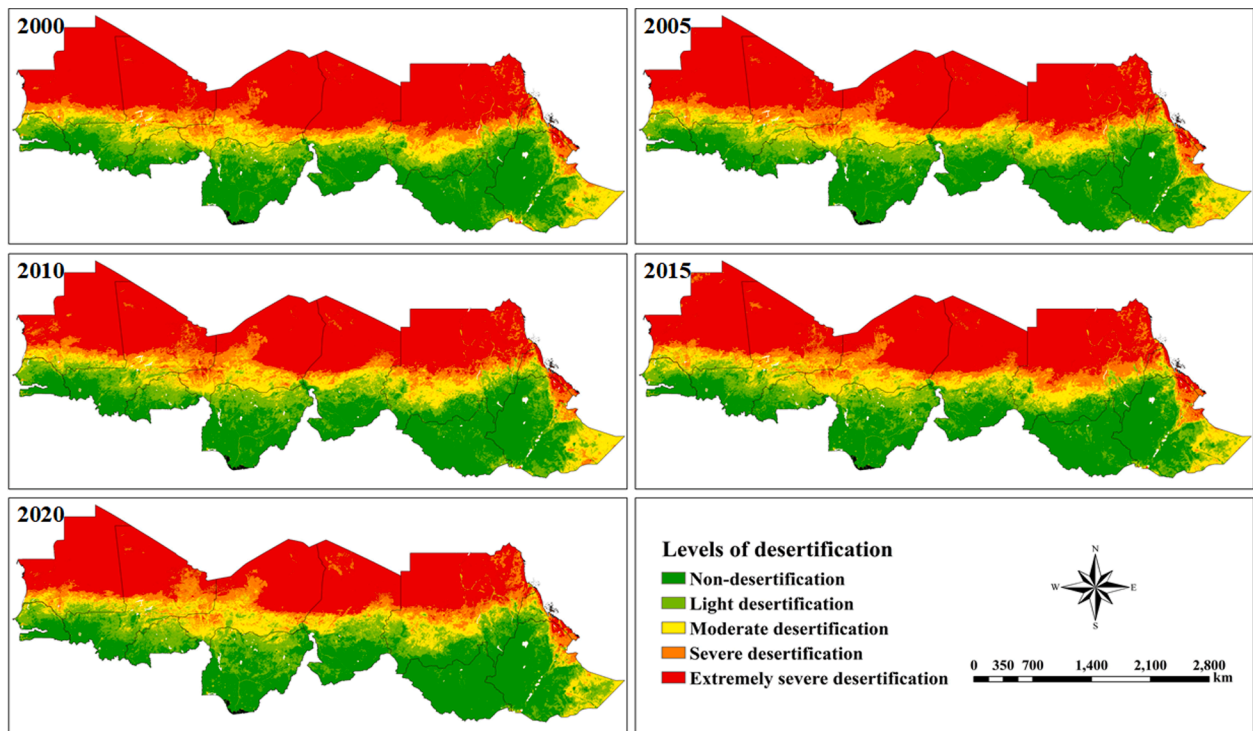
**Fig. 4.** Spatial distribution of desertification in the Sahel during 2000–2020.
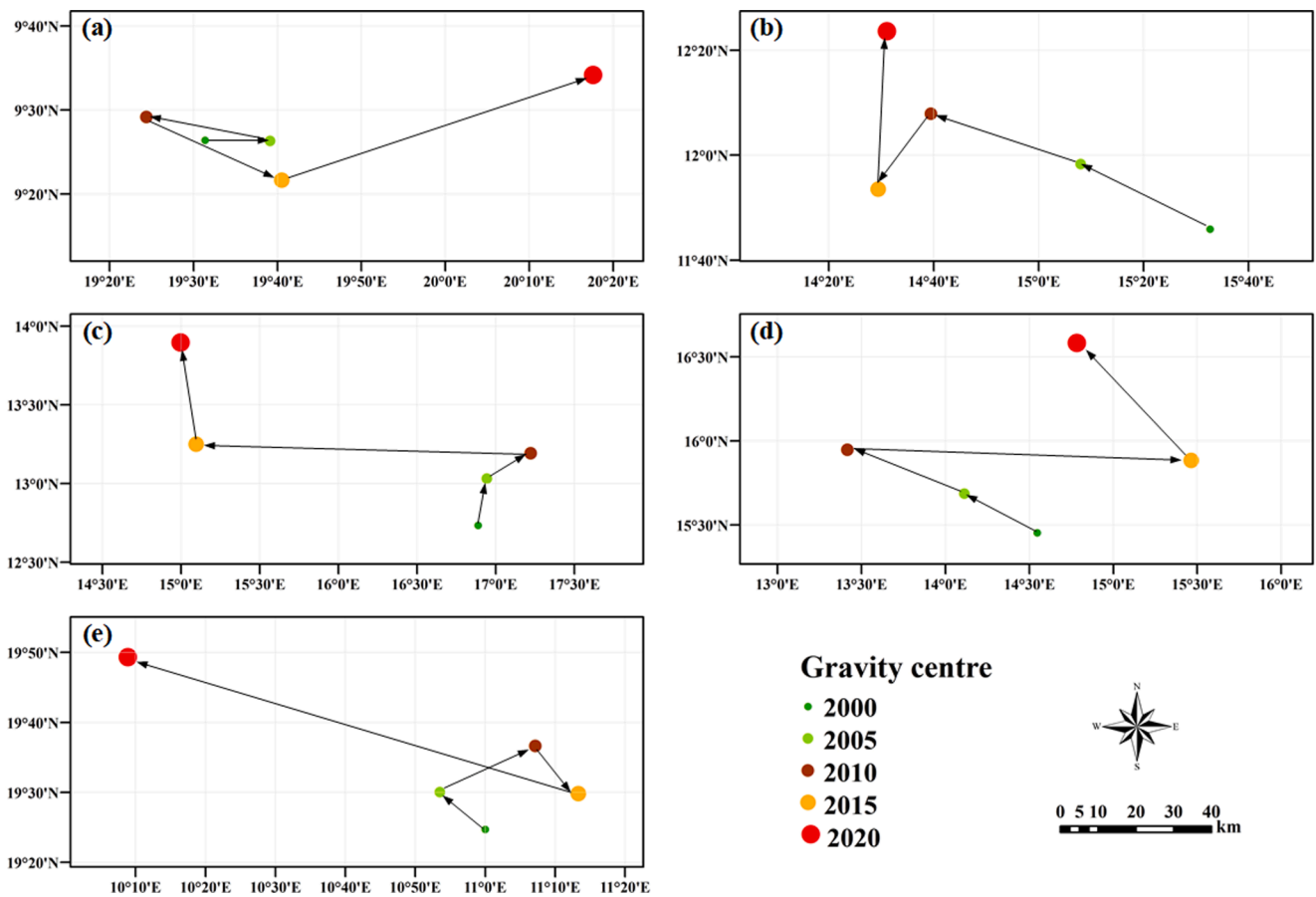


**Fig. 5.** Gravity centre migration of different desertification levels: (a) none, (b) light, (c) moderate, (d) severe, and (e) extremely severe.
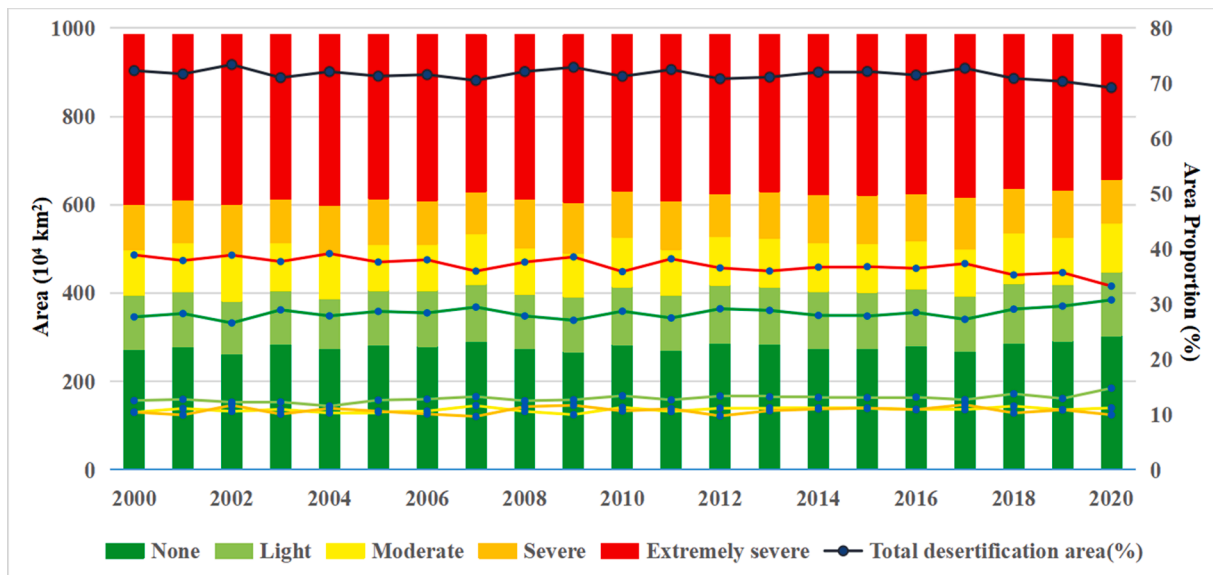
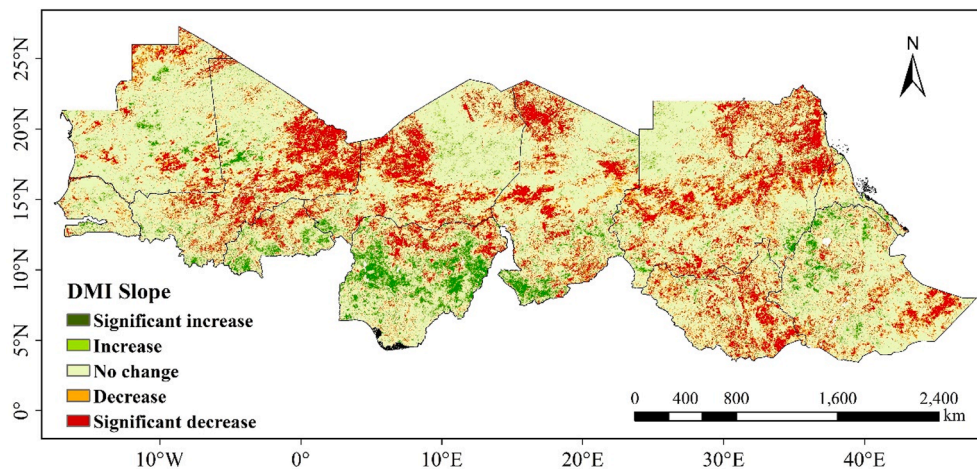**Fig. 6.** Area changes of different desertification levels in the Sahel, 2000–2020.



**Fig. 7.** Change trend of DMI (desertification monitoring index) in the Sahel, 2000–2020.
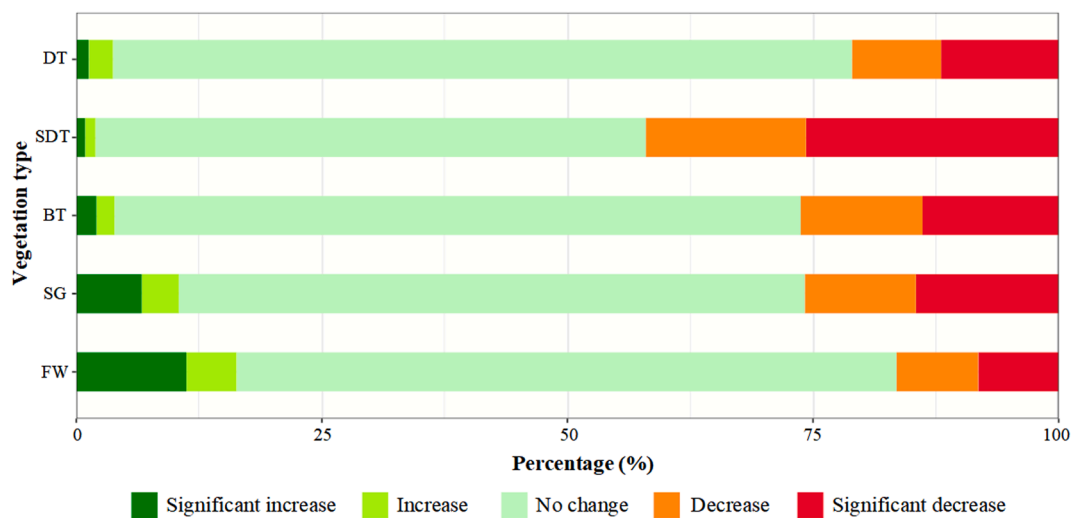


**Fig. 8.** Percentage of DMI changes across different vegetation types: DT, Desert; SDT, Semidesert; BT, Bushland and thicket; SG, Savanna grassland; FW, Forest and woodland.
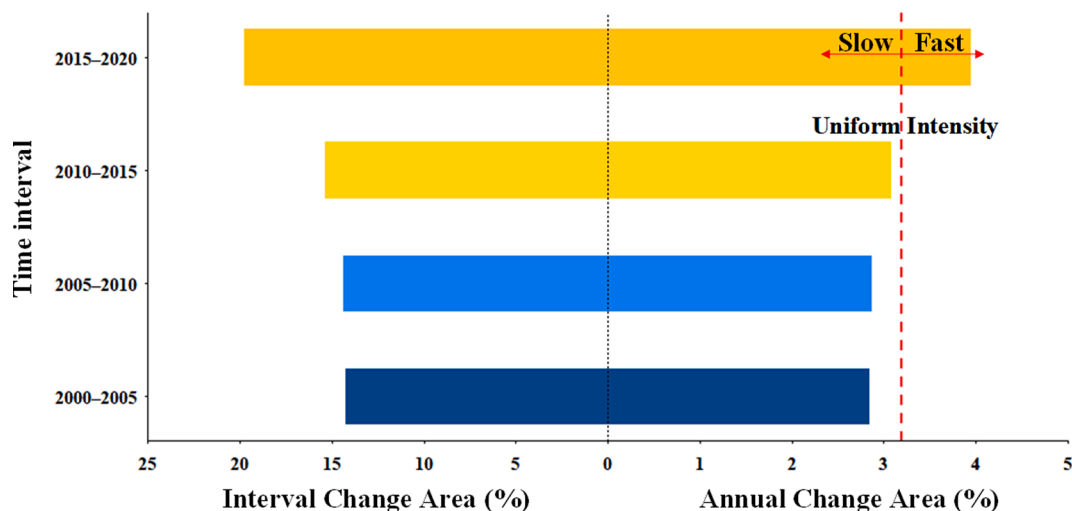
**Fig. 9.** Results from the time interval intensity analysis, where the left side represents the proportion of the area where the desertification categories changed in each period, and the right side represents the intensity of annual variability. The dotted red line depicts the proportion of average change over the years (uniform line).

### 3.2.2. Temporal variation

From the statistical analyses of desertification level areas (Fig. 6), it was found that the total desertification area (light, moderate, severe, and extremely severe) decreased from 72.31% ($712.56*10^4$ km$^2$) to 69.23% ($682.21*10^4$ km$^2$) over the analysis period. Overall, the total desertification area has remained relatively unchanged; however, extremely severe desertification area has substantially dropped from 38.92% ($383.48*10^4$ km$^2$) to 33.27% ($327.84*10^4$ km$^2$); whereas all other forms of desertification have either remain unchanged, or shown a fluctuating upward trend. The area of non-desertification, conversely, has increased from 27.69% to 30.77%.

To further analyse the temporal changes of desertification levels in the Sahel, the slope trend and significance results of each pixel were obtained through iterative regression calculations (Fig. 7). It was found that 18.47% of the Sahel regions underwent significant changes in DMI, while the remaining 81.53% showed insignificant or no change. DMI was significantly reduced in 14.59% of the regions, primarily

concentrated in the Aïr Massif, Adrar des Ifoghas, Tibesti Mountains, and widely throughout Sudan and South Sudan. The main reason for this distribution was likely to the increase in vegetation productivity with greater precipitation across the Sahel (Kaptué et al., 2015). The regions with a significant increase in DMI accounted for only 3.88%, which were concentrated in Nigeria, southern Chad, and parts of Ethiopia. Anthropogenic activities, such as agricultural reclamation and overgrazing, may be primary driver of these deepening desertification patterns in these regions (Nwilo et al., 2020).

There were notable differences in the desertification processes of different vegetation types across the Sahel (Fig. 8). The forest and woodland areas of upward and downward DMI trends were nearly equal, accounting for 16.3% and 16.5% of the total area, respectively; however, the significantly increased area of DMI was larger than the significantly decreased area, indicating that the forests in parts of the Sahel have been severely damaged and desertified. The DMI of the savanna grassland area showed an increasing trend across 10.43% of the
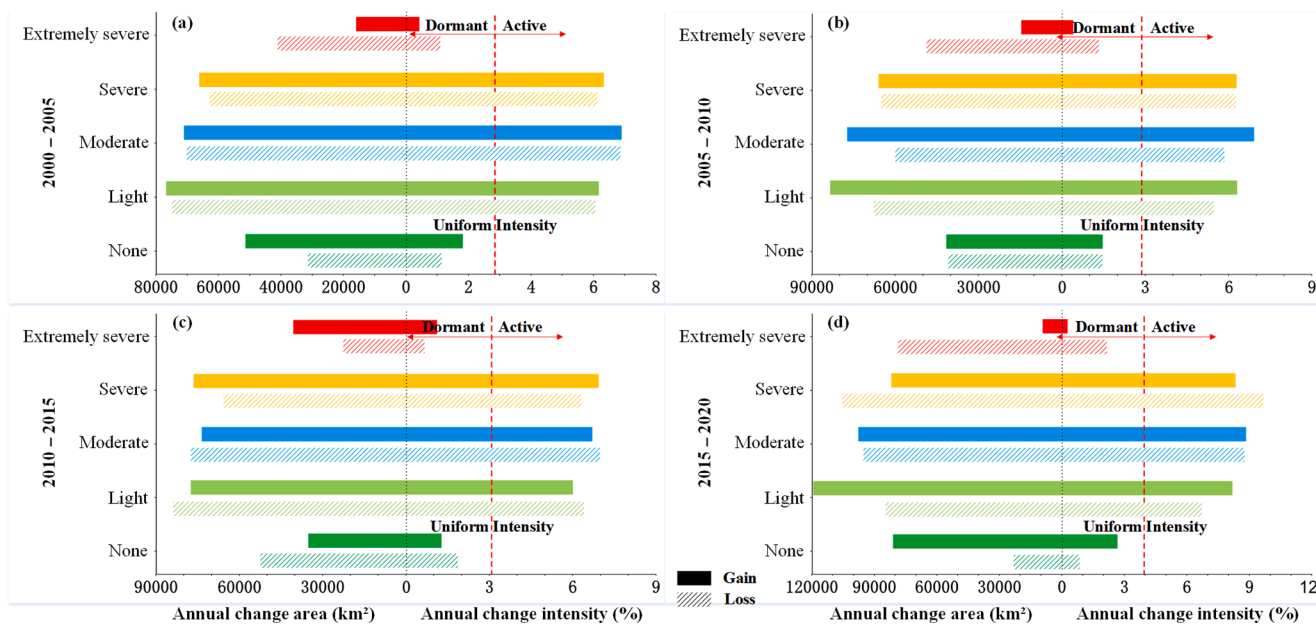


**Fig. 10.** Category intensity analysis for the four-time intervals: (a) 2000–2005, (b) 2005–2010, (c) 2010–2015, (d) 2015–2020. Bars extending to the left of zero show gross annual area gains and losses across the study region, while bars extending to the right of zero show the intensity of annual gains and losses within each category.

**Table 4**
Categorical and area (km$^2$) conversions over each time interval analysed.

| From | To | 2000–2005 | | 2005–2010 | | 2010–2015 | | 2015–2020 | |
|---|---|---|---|---|---|---|---|---|---|
| *None* | Category | Light | \ | Light | \ | Light | \ | Light | \ |
| | Area | 31,137 | \ | 40,308 | \ | 50,820 | \ | 23,158 | \ |
| *Light* | Category | Moderate | None | Moderate | None | Moderate | None | None | \ |
| | Area | 24,763 | 49,387 | 26,650 | 40,767 | 45,736 | 34,766 | 74,859 | \ |
| *Moderate* | Category | Light | Severe | Light | Severe | Severe | Light | Light | |
| | Area | 43,011 | 25,360 | 41,131 | 17,940 | 50,213 | 25,803 | 82,360 | |
| *Severe* | Category | Moderate | \ | Moderate | | Moderate | Extremely severe | Moderate | |
| | Area | 44,508 | \ | 48,863 | \ | 25,896 | 39,272 | 82,241 | |
| *Extremely severe* | Category | Severe | \ | Severe | \ | Severe | \ | Severe | \ |
| | Area | 39,935 | \ | 47,556 | \ | 22,448 | \ | 73,426 | \ |

total area, and decreasing trend across 25.85%. The significantly decreased areas were also greater than the significantly increasing areas, indicating an overall decrease in desertification levels of the savanna from 2000 to 2020. Directionally, the shrub and semi-desert vegetation trends were similar to that of the savanna; however, the decreasing DMI trends were much more prominent than the upward trends, resulting in a significantly decreasing level of desertification in these regions. The DMI of desert areas also had an overall downward trend greater than the upward, leading to a decreasing area of extremely severe desertification as well.

The above analyses showed that the desertification in the Sahel has been improving overall, largely due to more conducive natural conditions over recent decades leading to a decrease in extremely severe desertification area; however, the levels of light, moderate, and severe desertification in areas with frequent anthropogenic activities are still increasing.

### 3.3. Intensity analysis of desertification

#### 3.3.1. Interval level analysis

Based on the method of intensity analysis, changes in desertification at various levels and time periods were explored. Interval intensity was used to analyse the change in area and intensity of land desertification level from 2000 to 2020 (Fig. 9). Over the entire analysis period, desertification intensity in the Sahel has increased, moving slowly from 2000 to 2015, and more rapidly from 2015 to 2020. By comparing the changes in intensity across the four time intervals, it was found that only the values during 2015–2020 were above average (uniform intensity = 3.19) over the entire study period, indicating a relatively rapid change intensity of desertification during this time interval compared to the last years. Indeed, the change in area was proportional to the intensity change (Fig. 9), increasing overall from 2000 to 2020, more from 2015 to 2020 than 2000 to 2015.

#### 3.3.2. Category level analysis

Fig. 10 shows the category level analysis results of the four time intervals. The change areas on the left side of the figure indicate that the gains and losses of light, moderate, and severe desertification land areas within each time interval were large; whereas changes in non-desertification and extremely severe desertification land areas were comparatively small. From 2000 to 2010, the gain area of non-desertification land was larger than the loss area, and the loss area of extremely severe desertification land was larger than the gain area. These patterns of desertification were reversed from 2010 to 2015, prior to improving again from 2015 to 2020. Overall, the gain of severe and extremely severe desertification land was less than the loss area, and the gain of non-desertification and light desertification land was greater than the loss area.

The right side of Fig. 10 indicates whether the area change was due to the larger categorical area, or the greater intensity of change within
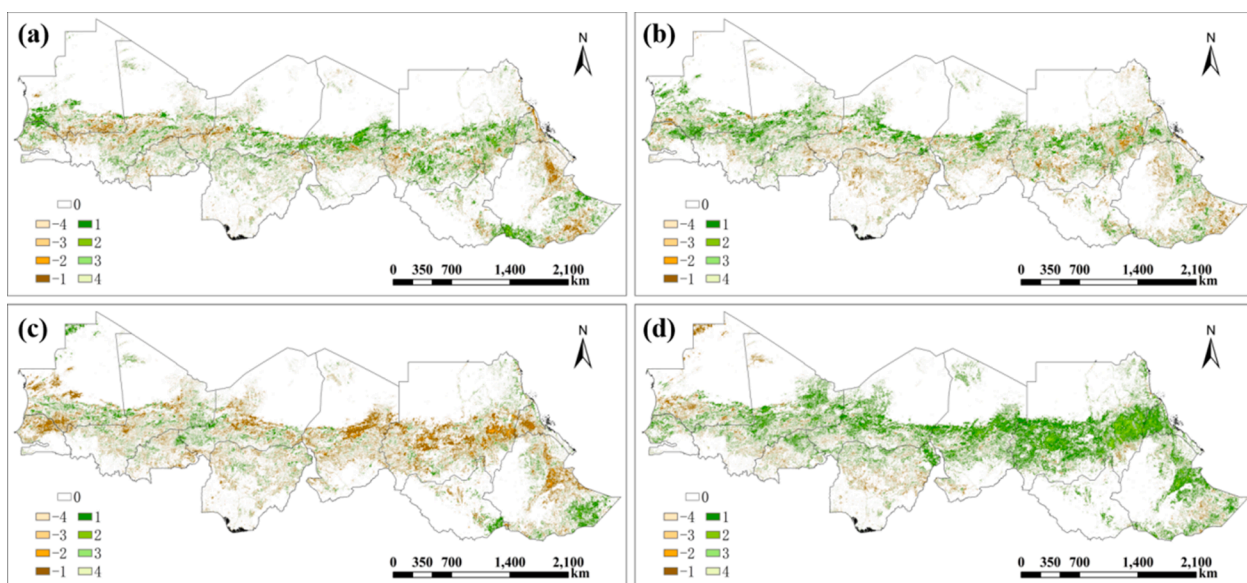


**Fig. 11.** Desertification level category changes in the Sahel, 2000–2020. (a) 2000–2005; (b) 2005–2010; (c) 2010–2015; (d) 2015–2020. Here, -1, -2, -3, and -4 represent the aggravation level of desertification, and the smaller the number, the greater the level of aggravation is. 1, 2, 3, and 4 indicate the levels of desertification mitigation, and the greater the value, the greater the level of desertification mitigation is.

**Table 5**
The *q* and *p* values for all factors of DMI distribution.

| Factors | PRE | LUT | WS | SM | PET | VT | LD | ST | TEM | ELEV | SLOP | ASP |
|---|---|---|---|---|---|---|---|---|---|---|---|---|
| *q* | 0.9269 | 0.8135 | 0.8068 | 0.788 | 0.7844 | 0.6767 | 0.5817 | 0.3506 | 0.1293 | 0.0975 | 0.0314 | 0.0048 |
| *p* | 0.000 | 0.000 | 0.000 | 0.000 | 0.000 | 0.000 | 0.000 | 0.000 | 0.000 | 0.000 | 0.000 | 0.000 |

Note: Precipitation (PRE), Temperature (TEM), Potential evapotranspiration (PET), Wind speed (WS), Elevation (ELEV), Slope (SLOP), Aspect (ASP), Vegetation type (VT), Soil type (ST), Soil moisture (SM), Livestock density (LD), Land use type (LUT).

the category. Accordingly, the gain and loss intensity of light, moderate, and severe desertification land were active over all time intervals (i.e., more than uniform intensity line); whereas non-desertification and extremely severe desertification land were in a dormant state (i.e., less than uniform intensity line). Thus, it was concluded that the former categories (light, moderate, and severe desertification land) are more sensitive to climate change and anthropogenic activities, and they are more likely to undergo mutual conversion compared to the more stable non-desertification and extremely severe desertification environments. Overall, levels of desertification has decreased from 2000 to 2020, primarily manifested as a decrease in extremely severe desertification, and an increase in non-desertification and light desertification areas.

### 3.3.3. Transition level analysis

The main transformation types and areas by level for each interval period were listed according to whether their transition intensity was above or below average (Table 4). At each time interval, non-desertification areas primarily transformed into light desertification, with the conversion increasing from 2000 to 2015, and decreasing from 2015 to 2020 (23,158 km$^2$). During 2000–2015, both light and moderate desertification experienced a two-way transformation, which tended to be higher and lower, respectively. Over the same period, light desertification mainly transformed into non-desertification (74,859 km$^2$), and moderate desertification largely transformed into light desertification (82,360 km$^2$). Severe desertification mostly transformed into moderate desertification; however, an area of 39,272 km$^2$ was transformed into extremely severe desertification during 2010–2015. As each interval, extremely severe desertification primarily transformed into severe desertification, and this transformed area has increased during 2000–2015 (73,426 km$^2$). Overall, the level of desertification has improved from 2000 to 2020, and the area of transformation from higher to lower levels was greater than that of the inverse. The area of extremely severe desertification was greatly reduced, and the total area transformed from severe desertification to extremely severe desertification was 39,272 km$^2$, and the total area transformed from extremely severe desertification to severe desertification was 182,365 km$^2$. The change level of the former is more than 4.5 times lower than that of the latter.

Fig. 11 depicts the spatial distribution of the transition intensity between the desertification levels in the Sahel at each time interval. The
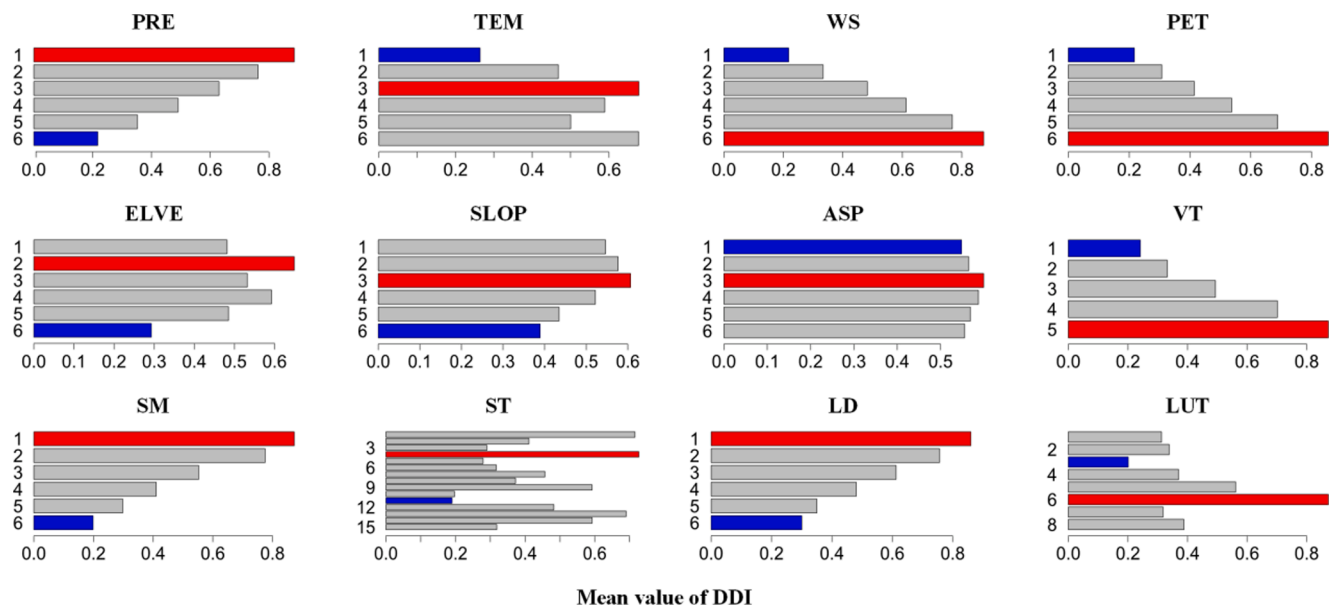
level of desertification in the northern deserts, southern forests, and Ethiopian plateau remained nearly unchanged throughout the study periods. The region of largest fluctuation was distributed in the central study area, indicating that this region is more sensitive to climate change and anthropogenic activities. Cross-level changes mainly occurred at two adjacent levels: none to light desertification, and moderate to light desertification, with few areas of cross-multilevel transformation. During 2000–2010, the level of desertification has reduced; whereas from 2010 to 2015, most areas have shifted towards an increase in desertification levels, which likely driven by the 2012 drought in the Sahel (Boyd et al., 2013). Following this incident, the extent of desertification has improved over a wider area during 2015–2020 as the climate maintained relatively normalcy.

### 3.4. Driving factors of desertification

#### 3.4.1. Single factor detection

The geographic detector model was used to attribute the spatial differentiation characteristics of the DMIs (Table 5). The factors were ranked according to their ability to explain the spatial differentiation characteristics of the observed DMI patterns: PRE > LUT > WS > SM > PET > VT > LD > ST > TEM > ELEV > SLOP > ASP. Moreover, all driving factors affecting the spatial differentiation of DMI were significant (*p* less than 0.05). The Sahel is located in the largest tropical arid zone; accordingly, precipitation factor dominates the spatial distribution of desertification in this area. Lying at the southern end of the Sahara Desert, wind speed also significantly affects the process of aeolian desertification. The *q* values of soil moisture, potential evapotranspiration, vegetation type, and livestock density were all greater than 0.5.

Although these values indicate that types of vegetation and soil have a high correlation with DMI, their relationship with desertification is not overly simple. The tropical study area experiences a relatively homogenous temperature across the east-west direction, save for in the Ethiopian Plateau area; accordingly, the spatial differentiation of temperature on the distribution of DMI throughout the Sahel is relatively small. Elevation, slope, and aspect affect the growth of vegetation through controlling local temperature conditions; however, because of temperature's small *q* value, factors such as elevation, slope, and aspect have the least influence on DMI distribution. Notably, the *q* values of anthropogenic activities—livestock density and land use type were

**Table 6**
Interactive detector and ecological detector matrix.

| | PRE | TEM | WS | PET | ELEV | SLOP | ASP | VT | SM | ST | LD | LUT |
|---|---|---|---|---|---|---|---|---|---|---|---|---|
| **PRE** | 0.9269 | Y | Y | Y | Y | Y | Y | Y | Y | Y | Y | Y |
| **TEM** | 0.9293 | 0.1293 | Y | Y | Y | Y | Y | Y | Y | Y | Y | Y |
| **WS** | 0.9316 | 0.819 | 0.8068 | Y | Y | Y | Y | Y | Y | Y | Y | Y |
| **PET** | 0.932 | 0.8332 | 0.8363 | 0.7844 | Y | Y | Y | Y | Y | Y | Y | Y |
| **ELEV** | 0.9302 | 0.1968 | 0.815 | 0.7984 | 0.0975 | Y | Y | Y | Y | Y | Y | Y |
| **SLOP** | 0.9284 | 0.1671 | 0.8118 | 0.7982 | 0.1187 | 0.0314 | Y | Y | Y | Y | Y | Y |
| **ASP** | 0.9273 | 0.1387 | 0.8091 | 0.7877 | 0.1054 | 0.0369 | 0.0048 | Y | Y | Y | Y | Y |
| **VT** | 0.9286 | 0.7354 | 0.8806 | 0.8644 | 0.7443 | 0.6923 | 0.6786 | 0.6767 | Y | Y | Y | Y |
| **SM** | 0.9379 | 0.8141 | 0.8759 | 0.852 | 0.7962 | 0.7933 | 0.7886 | 0.8659 | 0.788 | Y | Y | Y |
| **ST** | 0.9321 | 0.4481 | 0.8256 | 0.799 | 0.423 | 0.3673 | 0.3571 | 0.7652 | 0.8078 | 0.3506 | Y | Y |
| **LD** | 0.9338 | 0.657 | 0.8665 | 0.859 | 0.612 | 0.5914 | 0.5828 | 0.7807 | 0.8824 | 0.716 | 0.5817 | Y |
| **LUT** | **0.944** | 0.8492 | 0.908 | 0.9061 | 0.8307 | 0.8195 | 0.8142 | 0.8685 | 0.921 | 0.8568 | 0.8415 | 0.8135 |

Note: Precipitation (PRE), Temperature (TEM), Potential evapotranspiration (PET), Wind speed (WS), Elevation (ELEV), Slope (SLOP), Aspect (ASP), Vegetation type (VT), Soil type (ST), Soil moisture (SM), Livestock density (LD), Land use type (LUT).

**Fig. 12.** Average DMI of driving factors in each level. 1–6 represent the six levels. But in particular, vegetation types are divided into 5 levels, soil types are divided into 15 levels, and land use types are divided into 8 levels. The red bar indicates that this level is most likely to have a higher DMI, and the blue bar indicates that this level has the least DMI.

0.8135 and 0.5817, respectively, indicating their strong influence on the distribution of desertification throughout the Sahel.

### 3.4.2. Interaction detection

Desertification is not the result of a single impact factor, but the synergistic interaction of multiple unique factors. The factors combination with the strongest interaction was precipitation and land use type (Table 6), with a $q$ value of 0.944; thus, pointing to the joint effects of desertification from both climatic and anthropogenic factors. Further, the combination of precipitation and other factors produced higher $q$ values. As stated, topographic factors affect temperatures, and their combinations reflected a stronger nonlinear-enhance, such as "TEM ∩ SLOP = 0.1671 > TEM (0.1293) + SLOP (0.0314)". Additionally, a nonlinear-enhance interaction was seen between aspect and most factors, save for the slope & aspect interaction's $q$ value, which was the lowest among all factors ($q = 0.0048$). Through ecological detector, all environmental factors have passed the significance test (Table 6), which indicates significant differences between all environmental factors.

### 3.4.3. Risk detection

Desertification risk detection was used to determine the driving factors across a specific time interval that could produce higher DMIs (Fig. 12). Understanding the extent of desertification risks helps identify the mechanisms controlling its occurrence and development, as well as target combative measures. The mean DMI value decreased with an increase in precipitation and soil moisture. The first level (PRE ≤ 133 mm) was the area with the highest DMI, while the sixth level (PRE greater than 706 mm) maintained the lowest. The monotonic decrease in DMI with precipitation and soil moisture further supports the dominant role of hydrological parameters in desertification. Wind speed and potential evapotranspiration were also important, positively correlated factor with DMI. Specifically, with conditions of WS > 3.24 m·s⁻¹ and PET > 2444 mm, the risk of desertification is greater. As the overall temperature across the Sahel is relatively stable, the temperature range associated with the highest risk of desertification was primarily distributed in the third level (23.7℃ < TEM ≤ 26.2℃), where the mean DMI was ≤ 0.6783. The topographic condition factors held little influence on the spatial differentiation of desertification, so the mean DMI values were relatively unchanged. However, vegetation and soil type were highly correlated with DMI. Aridosols and Arenosols had the

highest average DMI values (0.7270 and 0.6903, respectively), as did desert vegetation (0.8725). Livestock density and land use type were also highly consistent with the spatial differentiation of DMIs, where areas with high mean DMI maintained lower livestock densities, and the values with high mean DMI were primarily located in unused land areas.

## 4. Discussion

### 4.1. Desertification monitoring method and accuracy verification

A large number of data were missing due to cloud and fog pollution in the high spatial resolution Landsat data in the tropics and the defects of the sensor itself. Therefore, MODIS data with complete data quality was selected for remote sensing monitoring of desertification in the Sahel. However, the medium spatial resolution MODIS data was prohibited extraction of finer details (Duan et al., 2019). For example, the nbon both sides of a desert river were pretty, but the distribution range was relatively small. Such details cannot be reflected in the medium-resolution MODIS data, and the area was incorrectly classified as desertification land. In the future, Landsat data can be used for more detailed research in small areas with frequent changes in desertification level in the Sahel. Here, only four reference variables-NDVI, MSAVI, albedo, and TGSIwere selected for the construction of a desertification monitoring model. More variables can be considered in the future to identify a more efficient feature space model that better reflects desertification changes in the Sahel (Guo et al., 2020). In the method of desertification remote sensing monitoring, machine learning methods can construct a relationship model between each index factor and desertification information to fit their non-linear relationships, potentially generating desertification assessment models with higher generalisation ability (Lamchin et al., 2016). Meng et al. (2021b) used six machine learning methods to classify the level of desertification in Mongolia, finding that the maximum entropy model had the highest accuracy. In the future, machine learning method can be used to monitor desertification in the Sahel, and the suitability of feature space model and machine learning model in the Sahel can be compared.

Previous studies have primarily used indicators, such as soil moisture, vegetation coverage, or land cover, for indirect verification of desertification level (Wei et al., 2018); and direct verification through the use of Landsat true colour synthesis images, or Google Earth high-
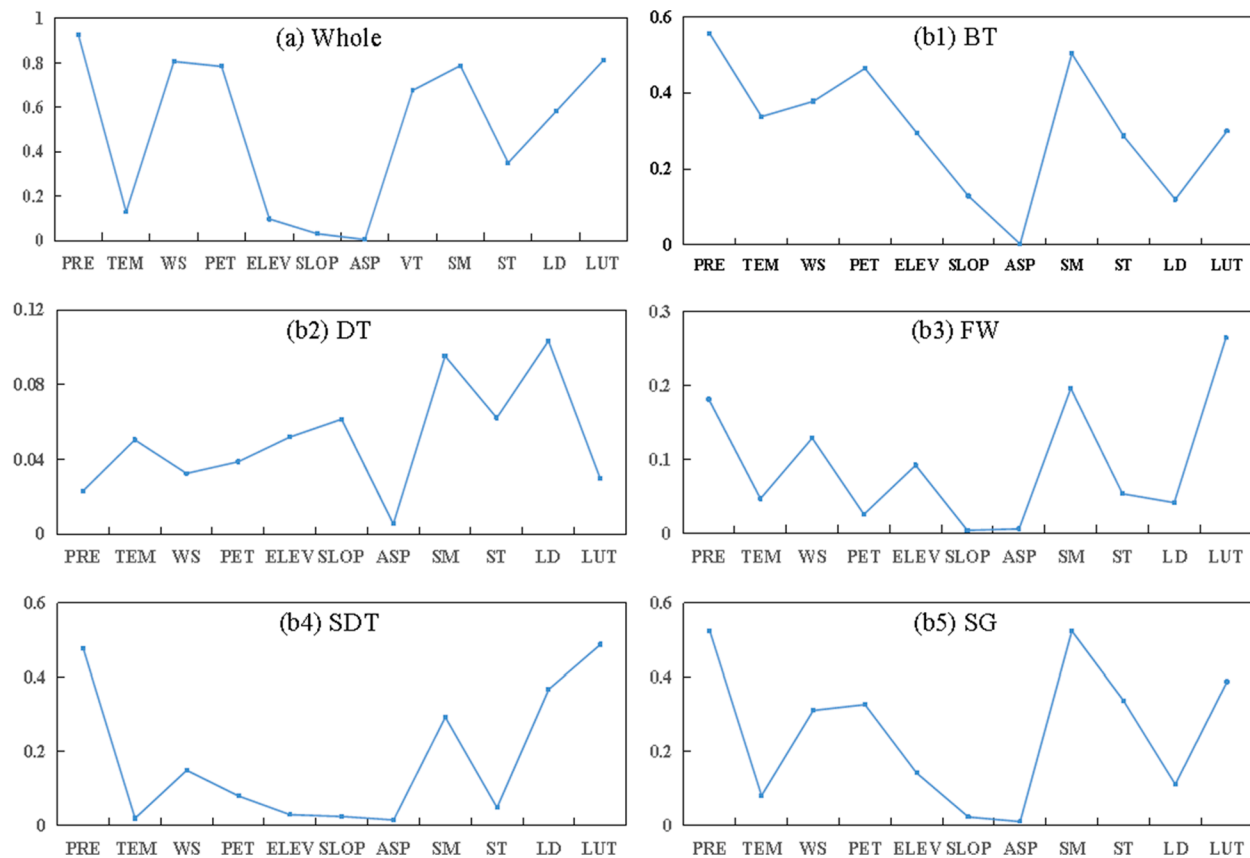
**Fig. 13.** Variations of q values for environmental factors on DMI distribution in Sahel: (a) as a whole, and (b1-b5) for different vegetation types (BT: Bushland and thicket; DT: Desert; FW: Forest and woodland; SDT: Semidesert; SG: Savanna grassland).

resolution imagery (Meng et al., 2021b), although verification results based on field survey data remains the most reliable (Qi et al., 2019). Guo et al. (2020) cross-verified the desertification monitoring results through Google Earth imagery and field observations, improving the reliability of the desertification monitoring model. Due to the impact of COVID-19, the field investigation portion of the present research was postponed, and the results of desertification monitoring in the Sahel were solely verified through Google Earth Landsat imagery, with an accuracy of 86.78%.

*4.2. Further analyses of desertification driving factors*

Under different spatial resolutions, the ability of each driving factor to interpret DMI is different. Moreover, in order to ensure the smooth operation of the geographic detector, all data need to be resampled to a consistent spatial resolution. In fact, the spatial differences of variables have been changed, which will have a certain impact on the final result. In the geographical detector, continuous variables must be discretized into categorical variables. Song et al. (2020) used a variety of traditional discretization methods for each $X$, and selected the optimal method according to the maximum $q$ value to improve the geographical detector; however, obtaining a globally optimal discretization result is never optimal when considering only the $X$ distribution, because $Y$ is ignored. Therefore, the research here adopted a multiscale discretization method that was improved by Meng et al. (2021a), where for $Y$, the information loss of the discrete $X$ obtained was minimized (i.e., $q$ value was maximized).

The research here analysed the driving factors of desertification levels throughout the Sahel (Fig. 13a), in which the spatial heterogeneity of the interior was neglected, but the factors across varying climatic zones, topographic regions, or vegetation types may differ (Meng

et al., 2020). The effect of driving factors on the spatial differentiation of DMI across vegetation types were compared (Fig. 13b1-b5), revealing that precipitation, soil moisture, and land use types were still the predominant factors for forests and woodlands, bushlands and thickets, savanna grasslands, and semi-desert vegetation areas, while topographical factors maintained little influence. While the effect of each factor on desert vegetation area was small, soil conditions and livestock density effects were high. In general, the dominant factors affecting the spatial differentiation of DMI in different vegetation types were still hydrological conditions and land use type, highlighting the issues of water and unsustainable land use that must be resolved for adequately managing Sahel desertification.

*4.3. Climate change and anthropogenic activities on desertification*

The Earth's changing climate is an important factor affecting the dynamic development of desertification. Precipitation was found here to be the primary driving factor controlling desertification in the Sahel. In the 1970 s and 1980 s, a reduction of precipitation in the Sahel resulted in moderate-to-severe drought, bringing about a deterioration of vegetation, and increased of desertification (Hein et al., 2011; Brandt et al., 2014). Tucker and Nicholson (1999) found that the vegetation boundary in the Sahel varied with precipitation, fluctuating less than or equal 150 km from north to south, highlighting the sensitivity of this region to climate change, and any correlated changes in precipitation. Thomas and Nigam (2018) found that the rain belt oscillated in the Sahel, and the Sahara's boundary line retreated northward during the rainy season, before expanding southward again during the dry season. Over the past 30 years, the vegetation coverage conditions in the Sahel have improved significantly, likely a result of the recovery of precipitation regimes after the great drought of the 1970 s and the 1980 s. The western Sahel has
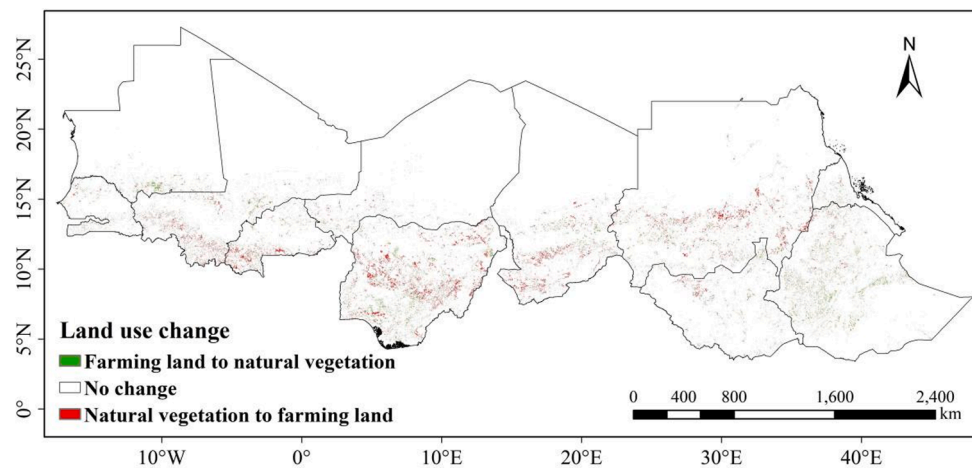
**Fig. 14.** Land use (farming land and natural vegetation) changing map in the Sahel.

become humid, total precipitation has been increasing, and the drought period was reduced. Overall, the Sahel has shown a state of re-greening, and reduced desertification, as evidenced by remote sensing observations revealing greater NDVI values due to increased vegetation coverage and reduced land degradation (Stith et al., 2016).

Notably, however, the spatial distribution of the re-greening did not perfectly align with trends of precipitation, and levels of desertification are still increasing in some areas (Herrmann et al., 2005). It is speculated that in addition to precipitation, the intensity of anthropogenic activities also impacts desertification dynamics. With human population growth, a corresponding increase in food demand and farmland is expected, both of which promote the use and conversion of natural forests and grasslands (D'Odorico et al., 2013; Bestelmeyer et al., 2015). Simultaneously, expanding agriculture has pushed animal husbandry areas north, into regions with poorer vegetation that are more susceptible to climate change and desertification. Indeed, Nwilo et al. (2020) found that the vegetation coverage in northern Nigeria widely decreased with no significant correlation to precipitation, but a strong negative correlation with population density and corresponding land degradation due to increased anthropogenic activities. Farmland in the Western Sahel has doubled since 1975, with settlement land has increased by a factor of 1.5 (Traore et al., 2014). Land use change maps of the Sahel from 2000 to 2020 identify the areas where natural vegetation is being converted into agricultural land mainly include southern Mali, most of Nigeria, southern Chad, and southern Sudan (Fig. 14). Notably, these areas have driven the increased levels of desertification under a general trend of reduction throughout the Sahel over the last 20 years.

The geographic detector model can be used to quantify the contribution of each influencing factor of desertification and the dominant factor affecting desertification can be identified. However, we did not have enough data on anthropogenic activities (for example, livestock data are only available in 2005 and 2010), and we cannot quantify the relationship between livestock density change and desertification index change by using geographic detector model, so it is unclear whether anthropogenic activity or climate change is more important to changes in the desertification level in the Sahel. This needs to be proved by collecting more and more comprehensive data.

## 5. Conclusions

Based on the surface parameters of NDVI, MSAVI, albedo, and TGSI generated by MODIS data from 2000 to 2020, different feature space models were constructed. The spatiotemporal variation was analysed by using the gravity centre migration method, slope trend analysis, and intensity analysis, and the driving factors of desertification were analysed via a geographical detector.

It was revealed that the point-to-point albedo-MSAVI model maintained the highest ability to extract desertification information in the Sahel, with an overall accuracy of 86.78%. From 2000 to 2020, the overall level of desertification in the Sahel has decreased: the area of extremely severe desertification has decreased from 38.92% ($383.48*10^4$ km$^2$) to 33.27% ($327.84*10^4$ km$^2$); whereas the area of non-desertification has increased from 27.69% to 30.77%. The regions with significantly reduced DMI accounted for 14.59%. Light, moderate, and severe desertification land was more sensitive to climate change and anthropogenic activities, and mutual transformation was frequent. Precipitation factors dominated the spatial distribution of desertification in the Sahel ($q$ value = 0.9269). The $q$ value of the two-factor, enhanced interaction of precipitation and land use type was 0.944, indicating that desertification is dependent upon both climate and anthropogenically derived activity.

Therefore, Sahelian countries should strengthen desertification control with the help of the international community in the aspects of the mitigation and adaptation of climate change, the restoration of degraded arid landscapes, and the guidance of local residents to sustainable use of forests and pastures.

## Authors' contributions

Zuowei Y conceived the study, analyzed the data, interpreted the findings, and prepared the manuscript under mentorship from Jiaqiang L. Xin G proposed the concept, interpreted the findings, contributed to the editing and reviewing of the manuscript. Xiaoyu M & Na Z provided guidance on research methods. All the authors read, revised, and approved the manuscript.

## Declaration of Competing Interest

The authors declare that they have no known competing financial interests or personal relationships that could have appeared to influence the work reported in this paper.

## Acknowledgements

## Appendix A. Supplementary data

Supplementary data to this article can be found online at https://doi.org/10.1016/j.catena.2022.106213.

## References

Aldwaik, S.Z., Pontius, R.G., 2012. Intensity analysis to unify measurements of size and stationarity of land changes by interval, category, and transition. Landsc. Urban Plan. 106 (1), 103–114. https://doi.org/10.1016/j.landurbplan.2012.02.010.

An, Y., Gao, W., Gao, Z., Liu, C., Shi, R., 2013. Assessment of desertification in the agro-pastoral transitional zone in Northern China (1982-2006) using GIMMS NDVI data. Rem. Sens. Model. Ecosyst. Sustain. X 8869, 181–190. https://doi.org/10.1117/12.2021857.

Benjaminsen, T.A., Hiernaux, P., 2019. From Desiccation to Global Climate Change: A History of the Desertification Narrative in the West African Sahel, 1900–2018. Global Environ. 12 (1), 206–236. https://doi.org/10.3197/ge.2019.120109.

Berrahmouni, N., Laestadius, L., Martucci, A., Mollicone, D., Patriarca, C., Sacande, M., 2016. Building Africa's Great Green Wall: Restoring Degraded Drylands for Stronger and More Resilient Communities. Food and Agriculture Organization of the United Nations, Rome, Italy.

Bestelmeyer, B.T., Okin, G.S., Duniway, M.C., Archer, S.R., Sayre, N.F., Williamson, J.C., Herrick, J.E., 2015. Desertification, land use, and the transformation of global drylands. Front. Ecol. Environ. 13 (1), 28–36. https://doi.org/10.1890/140162.

Boyd, E., Cornforth, R.J., Lamb, P.J., Tarhule, A., Lélé, M.I., Brouder, A., 2013. Building resilience to face recurring environmental crisis in African Sahel. Nat. Clim. Change 3 (7), 631–637. https://doi.org/10.1038/nclimate1856.

Brandt, M., Romankiewicz, C., Spiekermann, R., Samimi, C., 2014. Environmental change in time series – An interdisciplinary study in the Sahel of Mali and Senegal. J. Arid Environ. 105, 52–63. https://doi.org/10.1016/j.jaridenv.2014.02.019.

Brandt, M., Tucker, C.J., Kariryaa, A., Rasmussen, K., Abel, C., Small, J., Chave, J., Rasmussen, L.V., Hiernaux, P., Diouf, A.A., Kergoat, L., Mertz, O., Igel, C., Gieseke, F., Schöning, J., Li, S., Melocik, K., Meyer, J., Sinno, S., Romero, E., Glennie, E., Montagu, A., Dendoncker, M., Fensholt, R., 2020. An unexpectedly large count of trees in the West African Sahara and Sahel. Nature 587 (7832), 78–82. https://doi.org/10.1038/s41586-020-2824-5.

Cheng, L., Lu, Q., Wu, B., Yin, C., Bao, Y., Gong, L., 2018. Estimation of the Costs of Desertification in China: A Critical Review. Land Degrad. Dev. 29 (4), 975–983. https://doi.org/10.1002/ldr.2562.

D'Odorico, P., Bhattachan, A., Davis, K.F., Ravi, S., Runyan, C.W., 2013. Global desertification: Drivers and feedbacks. Adv. Water Resour. 51, 326–344. https://doi.org/10.1016/j.advwatres.2012.01.013.

Dardel, C., Kergoat, L., Hiernaux, P., Mougin, E., Grippa, M., Tucker, C.J., 2014. Re-greening Sahel: 30years of remote sensing data and field observations (Mali, Niger). Remote Sens. Environ. 140, 350–364. https://doi.org/10.1016/j.rse.2013.09.011.

Dawelbait, M., Morari, F., 2012. Monitoring desertification in a Savannah region in Sudan using Landsat images and spectral mixture analysis. J. Arid Environ. 80, 45–55. https://doi.org/10.1016/j.jaridenv.2011.12.011.

Dimobe, K., Ouédraogo, A., Soma, S., Goetze, D., Porembski, S., Thiombiano, A., 2015. Identification of driving factors of land degradation and deforestation in the Wildlife Reserve of Bontioli (Burkina Faso, West Africa). Global Ecol. Conserv. 4, 559–571. https://doi.org/10.1016/j.gecco.2015.10.006.

Du, Z., Xu, X., Zhang, H., Wu, Z., Liu, Y., 2016. Geographical Detector-Based Identification of the Impact of Major Determinants on Aeolian Desertification Risk. PLoS One 11. https://doi.org/10.1371/journal.pone.0151331.

Duan, H., Wang, T., Xue, X., Yan, C., 2019. Dynamic monitoring of aeolian desertification based on multiple indicators in Horqin Sandy Land, China. Sci. Total Environ. 650, 2374–2388. https://doi.org/10.1016/j.scitotenv.2018.09.374.

Fust, W., 2010. Human Impact Report: Climate Change–The Anatomy of a Silent Crisis. Global Humanitarian Forum, Geneva.

Giannini, A., Salack, S., Lodoun, T., Ali, A., Gaye, A.T., Ndiaye, O., 2013. A unifying view of climate change in the Sahel linking intra-seasonal, interannual and longer time scales. Environ. Res. Lett. 8 (2), 024010. https://doi.org/10.1088/1748-9326/8/2/024010.

Gou, F., Liang, W., Sun, S., Jin, Z., Zhang, W., Yan, J., 2021. Analysis of the desertification dynamics of sandy lands in Northern China over the period 2000–2017. Geocarto Int. 36 (17), 1938–1959. https://doi.org/10.1080/10106049.2019.1678677.

Guo, B., Wen, Y., 2020. An Optimal Monitoring Model of Desertification in Naiman Banner Based on Feature Space Utilizing Landsat8 Oli Image. IEEE Access 8, 4761–4768. https://doi.org/10.1109/access.2019.2962909.

Guo, B., Zang, W., Han, B., Yang, F., Luo, W., He, T., Fan, Y., Yang, X., Chen, S., 2020. Dynamic monitoring of desertification in Naiman Banner based on feature space models with typical surface parameters derived from LANDSAT images. Land Degrad. Dev. 31 (12), 1573–1592. https://doi.org/10.1002/ldr.3533.

Han, Z., Wang, T., Yan, C., Liu, Y., Liu, L., Li, A., Du, H., 2010. Change trends for desertified lands in the Horqin Sandy Land at the beginning of the twenty-first century. Environ. Earth Sci. 59 (8), 1749–1757. https://doi.org/10.1007/s12665-009-0157-7.

Hein, LARS, De ridder, NICO, 2006. Desertification in the Sahel: a reinterpretation. Glob. Change Biol. 12 (5), 751–758. https://doi.org/10.1111/j.1365-2486.2006.01135.x.

Hein, L., de Ridder, N., Hiernaux, P., Leemans, R., de Wit, A., Schaepman, M., 2011. Desertification in the Sahel: Towards better accounting for ecosystem dynamics in the interpretation of remote sensing images. J. Arid Environ. 75 (11), 1164–1172. https://doi.org/10.1016/j.jaridenv.2011.05.002.

Herrmann, S.M., Anyamba, A., Tucker, C.J., 2005. Recent trends in vegetation dynamics in the African Sahel and their relationship to climate. Global Environ. Change 15 (4), 394–404. https://doi.org/10.1016/j.gloenvcha.2005.08.004.

Houerou, H.N.L., 1980. The Rangelands of the Sahel. J. Range Manag. 33 (1), 41. https://doi.org/10.2307/3898226.

Hu, Y., Han, Y., Zhang, Y., 2020. Land desertification and its influencing factors in Kazakhstan. J. Arid Environ. 180, 104203. https://doi.org/10.1016/j.jaridenv.2020.104203.

Hua, D., Hao, X., 2021. Spatiotemporal change and drivers analysis of desertification in the arid region of northwest China based on geographic detector. Environ. Challenges 4, 100082. https://doi.org/10.1016/j.envc.2021.100082.

Jiang, L., Bao, A., Jiapaer, G., Guo, H., Zheng, G., Gafforov, K., Kurban, A., De Maeyer, P., 2019. Monitoring land sensitivity to desertification in Central Asia: Convergence or divergence? Sci. Total Environ. 658, 669–683. https://doi.org/10.1016/j.scitotenv.2018.12.152.

Kamuanga, M.J.B., Somda, J., Sanon, Y., Kagoné, H., 2008. Livestock and regional market in the Sahel and West Africa Potentials and challenges. SWAC-OECD/ECOWAS. https://www.oecd.org/swac/publications/41848366.pdf.

Kaptué, A.T., Prihodko, L., Hanan, N.P., 2015. On regreening and degradation in Sahelian watersheds. Proc. Natl. Acad. Sci. USA 112 (39), 12133–12138. https://doi.org/10.1073/pnas.1509645112.

Kremer, R.G., Running, S.W., 1993. Community type differentiation using NOAA/AVHRR data within a sagebrush-steppe ecosystem. Remote Sens. Environ. 46 (3), 311–318. https://doi.org/10.1016/0034-4257(93)90051-x.

Kundu, A., Patel, N.R., Saha, S.K., Dutta, D., 2017. Desertification in western Rajasthan (India): an assessment using remote sensing derived rain-use efficiency and residual trend methods. Nat. Hazards 86 (1), 297–313. https://doi.org/10.1007/s11069-016-2689-y.

Kusserow, H., 2017. Desertification, Resilience and Re-greening in the African Sahel – A matter of the observation period? Earth Syst. Dyn. Discuss. 1–33. https://doi.org/10.5194/esd-2017-4.

Lamchin, M., Lee, J.Y., Lee, W.K., Lee, E.J., Kim, M., Lim, C.H., Choi, H.A., Kim, S.R., 2016. Assessment of land cover change and desertification using remote sensing technology in a local region of Mongolia. Adv. Space Res. 57 (1), 64–77. https://doi.org/10.1016/j.asr.2015.10.006.

Leroux, L., Bégué, A., Lo Seen, D., Jolivot, A., Kayitakire, F., 2017. Driving forces of recent vegetation changes in the Sahel: Lessons learned from regional and local level analyses. Remote Sens. Environ. 191, 38–54. https://doi.org/10.1016/j.rse.2017.01.014.

Li, S., Zheng, Y., Luo, P., Wang, X., Li, H., Lin, P., 2007. Desertification in western Hainan Island, China (1959 to 2003). Land Degrad. Dev. 18 (5), 473–485. https://doi.org/10.1002/ldr.787.

Li, Y., Li, H., Xu, F., 2021. Spatiotemporal changes in desertified land in rare earth mining areas under different disturbance conditions. Environ. Sci. Pollut. Res. Int. 28 (23), 30323–30334. https://doi.org/10.1007/s11356-021-12476-x.

Meng, X., Gao, X., Lei, J., Li, S., 2021a. Development of a multiscale discretization method for the geographical detector model. Int. J. Geograph. Inform. Sci. 35 (8), 1650–1675. https://doi.org/10.1080/13658816.2021.1884686.

Meng, X., Gao, X., Li, S., Lei, J., 2020. Spatial and Temporal Characteristics of Vegetation NDVI Changes and the Driving Forces in Mongolia during 1982–2015. Remote Sens. 12 (4), 603. https://doi.org/10.3390/rs12040603.

Meng, X., Gao, X., Li, S., Li, S., Lei, J., 2021b. Monitoring desertification in Mongolia based on Landsat images and Google Earth Engine from 1990 to 2020. Ecol. Ind. 129, 107908. https://doi.org/10.1016/j.ecolind.2021.107908.

Mirzabaev, A.J., Wu, J., Evans, F., García-Oliva, I.A.G., Hussein, M.H., Iqbal, J., Kimutai, T., Knowles, F., Meza, D., Nedjraoui, F., Tena, M., Türkeş, R.J., Vázquez, M., 2019. Weltz. Desertification. In: Climate Change and Land: An IPCC Special Report on Climate Change, Desertification, Land Degradation, Sustainable Land Management, Food Security, and Greenhouse Gas Fluxes in Terrestrial Ecosystems. https://www.ipcc.ch/srccl/chapter/chapter-3/.

Na, R., Du, H., Na, L., Shan, Y., He, H., Wu, Z., Zong, S., Yang, Y., Huang, L., 2019. Spatiotemporal changes in the Aeolian desertification of Hulunbuir Grassland and its driving factors in China during 1980–2015. Catena 182, 104123. https://doi.org/10.1016/j.catena.2019.104123.

Niang, A.J., Ozer, A., Ozer, P., 2008. Fifty years of landscape evolution in Southwestern Mauritania by means of aerial photos. J. Arid Environ. 72 (2), 97–107. https://doi.org/10.1016/j.jaridenv.2007.04.009.

Nicholson, S.E., 2018. Climate of the Sahel and West Africa. Oxford Research Encyclopedia of Climate Science. https://doi.org/10.1093/acrefore/9780190228620.013.510.

Nwilo, P.C., Olayinka, D.N., Okolie, C.J., Emmanuel, E.I., Orji, M.J., Daramola, O.E., 2020. Impacts of land cover changes on desertification in northern Nigeria and implications on the Lake Chad Basin. J. Arid Environ. 181, 104190. https://doi.org/10.1016/j.jaridenv.2020.104190.

Policelli, F., Hubbard, A., Jung, H.C., Zaitchik, B., Ichoku, C., 2019. A predictive model for Lake Chad total surface water area using remotely sensed and modeled hydrological and meteorological parameters and multivariate regression analysis. J. Hydrol. 568, 1071–1080. https://doi.org/10.1016/j.jhydrol.2018.11.037.

Pye, N., White, F., 1985. The Vegetation of Africa: A Descriptive Memoir to Accompany the UNESCO/AETFAT/UNSO Vegetation Map of Africa. Geograph. J. 151 (1), 132. https://doi.org/10.2307/633318.

Qi, J., Chehbouni, A., Huete, A.R., Kerr, Y.H., Sorooshian, S., 1994. A modified soil adjusted vegetation index. Remote Sens. Environ. 48 (2), 119–126. https://doi.org/10.1016/0034-4257(94)90134-1.

Qi, X., Zhang, C., Wang, K., 2019. Comparing Remote Sensing Methods for Monitoring Karst Rocky Desertification at Sub-pixel Scales in a Highly Heterogeneous Karst Region. Sci. Rep. 9, 13368. https://doi.org/10.1038/s41598-019-49730-9.

Rasmussen, K., Brandt, M., Tong, X., Hiernaux, P., Diouf, A.A., Assouma, M.H., Tucker, C. J., Fensholt, R., 2018. Does grazing cause land degradation? Evidence from the sandy Ferlo in Northern Senegal. Land Degrad. Dev. 29 (12), 4337–4347. https://doi.org/10.1002/ldr.3170.

Siebert, A., 2014. Hydroclimate Extremes in Africa: Variability, Observations and Modeled Projections. Geography Compass 8 (6), 351–367. https://doi.org/10.1111/gec3.12136.

Song, Y., Wang, J., Ge, Y., Xu, C., 2020. An optimal parameters-based geographical detector model enhances geographic characteristics of explanatory variables for spatial heterogeneity analysis: cases with different types of spatial data. GIScience Remote Sens. 57 (5), 593–610. https://doi.org/10.1080/15481603.2020.1760434.

Sop, T.K., Oldeland, J., 2013. Local Perceptions of Woody Vegetation Dynamics in the Context of a 'Greening Sahel': A Case Study from Burkina Faso. Land Degrad. Dev. 24 (6), 511–527. https://doi.org/10.1002/ldr.1144.

Sterk, G., Stoorvogel, J.J., 2020. Desertification–Scientific Versus Political Realities. Land 9 (5), 156. https://doi.org/10.3390/land9050156.

Stith, M., Giannini, A., Corral, J.D., Adamo, S., de Sherbinin, A., 2016. A Quantitative Evaluation of the Multiple Narratives of the Recent Sahelian Regreening*. Weather Clim. Soc. 8 (1), 67–83. https://doi.org/10.1175/wcas-d-15-0012.1.

Thomas, N., Nigam, S., 2018. Twentieth-Century Climate Change over Africa: Seasonal Hydroclimate Trends and Sahara Desert Expansion. J. Clim. 31 (9), 3349–3370. https://doi.org/10.1175/jcli-d-17-0187.1.

Tierney, J.E., Ummenhofer, C.C., deMenocal, P.B., 2015. Past and future rainfall in the Horn of Africa. Sci. Adv. 1 (9) https://doi.org/10.1126/sciadv.1500682.

Traore, S.B., Ali, A., Tinni, S.H., Samake, M., Garba, I., Maigari, I., Alhassane, A., Samba, A., Diao, M.B., Atta, S., Dieye, P.O., Nacro, H.B., Bouafou, K.G.M., 2014. AGRHYMET: A drought monitoring and capacity building center in the West Africa Region. Weather Clim. Extremes 3, 22–30. https://doi.org/10.1016/j.wace.2014.03.008.

Tucker, C.J., Nicholson, S.E., 1999. Variations in the size of the Sahara Desert from 1980 to 1997. Ambio 28, 587–591.

Turan, İ.D., Dengiz, O., Özkan, B., 2019. Spatial assessment and mapping of soil quality index for desertification in the semi-arid terrestrial ecosystem using MCDM in interval type-2 fuzzy environment. Comput. Electron. Agric. 164, 104933. https://doi.org/10.1016/j.compag.2019.104933.

UNDP, 2019. Human Development Report 2019. Beyond Income, Beyond Averages. Beyond Today: Inequalities in Human Development in the 21st Century, 23. Oxford University Press, pp. 308–311.

Uzuner, Ç., Dengiz, O., 2020. Desertification risk assessment in Turkey based on environmentally sensitive areas. Ecol. Ind. 114, 106295. https://doi.org/10.1016/j.ecolind.2020.106295.

Verstraete, M.M., Pinty, B., 1996. Designing optimal spectral indexes for remote sensing applications. IEEE Trans. Geosci. Remote Sens. 34 (5), 1254–1265. https://doi.org/10.1109/36.536541.

Vorovencii, I., 2017. Applying the change vector analysis technique to assess the desertification risk in the south-west of Romania in the period 1984–2011. Environ. Monit. Assess 189, 524. https://doi.org/10.1007/s10661-017-6234-6.

Wang, J., Zhang, T., Fu, B., 2016. A measure of spatial stratified heterogeneity. Ecol. Ind. 67, 250–256. https://doi.org/10.1016/j.ecolind.2016.02.052.

Wang, X., Chen, F., Dong, Z., 2006. The relative role of climatic and human factors in desertification in semiarid China. Global Environ. Change 16 (1), 48–57. https://doi.org/10.1016/j.gloenvcha.2005.06.006.

Wei, H., Wang, J., Cheng, K., Li, G., Ochir, A., Davaasuren, D., Chonokhuu, S., 2018. Desertification Information Extraction Based on Feature Space Combinations on the Mongolian Plateau. Remote Sens. 10 (10), 1614. https://doi.org/10.3390/rs10101614.

Wu, Z., Lei, S., Bian, Z., Huang, J., Zhang, Y., 2019. Study of the desertification index based on the albedo-MSAVI feature space for semi-arid steppe region. Environ. Earth Sci. 78 (6) https://doi.org/10.1007/s12665-019-8111-9.

Xiao, J., Shen, Y., Tateishi, R., Bayaer, W., 2006. Development of topsoil grain size index for monitoring desertification in arid land using remote sensing. Int. J. Remote Sens. 27 (12), 2411–2422. https://doi.org/10.1080/01431160600554363.

Xu, D., Li, C., Zhuang, D., Pan, J., 2011. Assessment of the relative role of climate change and human activities in desertification: A review. J. Geog. Sci. 21 (5), 926–936. https://doi.org/10.1007/s11442-011-0890-1.

Xue, Z., Qin, Z., Cheng, F., Ding, G., Li, H., 2017. Quantitative assessment of aeolian desertification dynamics- A case study in north Shanxi of China (1975 to 2015). Sci. Rep. 7, 10460. https://doi.org/10.1038/s41598-017-11073-8.

Zeng, Y., Xiang, N., Feng, Z., Xu, H., 2006. Albedo-NDVI space and remote sensing synthesis index models for desertification monitoring. Sci. Geograph. Sin. 01, 75–81. https://doi.org/10.3969/j.issn.1000-0690.2006.01.013.